A full-field crystal-plasticity analysis of bimodal polycrystals

B. Flipon, Clément Keller, R. Quey, Fabrice Barbe

A full-field crystal-plasticity analysis of bimodal polycrystals

B. Flipon[a,*], C. Keller[a], R. Quey[b], F. Barbe[a,*]

[a] *Normandie Univ, INSA Rouen, UNIROUEN, GPM, UMR CNRS 6634, 76000 Rouen, France*
[b] *Mines Saint-Étienne, Univ Lyon, CNRS, UMR 5307 LGF, Centre SMS, F – 42023 Saint-Étienne, France*

Abstract

A full field crystal plasticity modelling of bimodal polycrystals is presented. Bimodal polycrystals are generated using a controlled Laguerre-Voronoi algorithm and a modified phenomenological law is used to take into account the grain size effect through a Hall-Petch term. A focus is particularly made on the effects of grain size and of grain size ratio between ultrafine grains and coarse grains populations on local and global mechanical responses. The effect of the spatial distribution of the coarse grains (clustered or isolated) is also analysed in terms of strain localisation and stress concentration at the local scale.

Key words:
Bimodal microstructure, Laguerre-Voronoi tessellations, Full-field crystal plasticity, Grain size effect

Contents

*Corresponding author
Email addresses: baptiste.flipon@insa-rouen.fr (B. Flipon), clement.keller@insa-rouen.fr (C. Keller), romain.quey@mines-stetienne.fr (R. Quey), fabrice.barbe@insa-rouen.fr (F. Barbe)

List of Figures

List of Tables

1. Introduction

It is well-known that decreasing the grain size (GS) of metallic alloys increases their yield stress (and mechanical strength), as described by the simple Hall-Petch law and observed nearly independently of the elaboration process [2, 3, 4, 5]. This has made GS reduction one of the most efficient way to increase the strength of metallic alloys and, as a result, reduce the weight of components, e.g. in the transportation industry. Higher strength, however, generally comes with lower ductility [6, 7], which is detrimental to formability or fracture resistance. Still, good combinations of strength and ductility can be obtained with specific microstructures, as reviewed by Ma in [8]. Nanotwinned copper [9] and nanostructured metals with second-phase precipitates are examples of materials with enhanced strain hardening [10, 11]. Polycrystals with a bimodal GS distribution (simply refered to as "bimodal polycrystals" in the following) also have attracted much interest, as their ultra-fine grains (UFG) can provide high mechanical strength while their coarse grains (CG) can provide ductility [12, 13, 14]. However, the mechanical properties of these materials remain delicate to control (and predict), as they depend not only on the grain size of the two populations, but also on their relative spatial distributions.

Several methods have been proposed to elaborate bimodal polycrystals, such as rolling and annealing [15, 16, 17], severe plastic deformation [18], or powder metallurgy combined to conventional or spark plasma sintering (SPS) [19, 13, 17, 20]. However, only the latter (and especially SPS) provides the direct, accurate control on the GS statistics (size distributions and volume fractions) required for analysing microstructure-property relationships in detail (although the amount of materials produced by SPS is much smaller than for deformation-based processes). Using this specific sintering route, the authors recently reported the influence of a bimodal distribution on the mechanical properties of 316L samples [20]. In particular an improvement of the strain to failure for a given yield stress has been observed for bimodal grain size distribution due to a modification of the backstress. However, these results seem to depend on the grain size ratio between each grain population, their respective average size and volume fraction, which raises several questions: What are the optimal properties of the powder, in terms of the grain sizes of the two populations and their relative volume fractions? What is the influence of their spatial distributions? These questions would be rather delicate and very time-consuming to answer experimentally, but are easily accessible to numerical simulations. Moreover, the simulation approach offers access not only to the macroscopic response of the material (yield stress, ductility), but also to its local response, i.e., the stress and strain distributions among and within grain populations, which is essential to a better understanding of all mechanisms at play.

The first-order description of a bimodal microstructure includes the mean GSs and volume fractions of the grain populations, as in a two-phase composite mean field approach. This description was adopted in the secant Mori-Tanaka mean field approach of Joshi *et al.* [21] to predict the effect of extrusion on the yield strength anisotropy and to analyse the effect of the CG volume fraction. In the biphase mean-field approach of Zhu *et al.* [22, 23], the scale transition was based on the model of Weng [24], and the two grain populations were assigned different constitutive behaviors: for the CG, the flow stress was mainly governed by intragranular dislocation storage and annihilation (as in the Kocks-Mecking model) while for the fine grains, the strain gradients were considered as stored in the grain boundary dislocation pile-up zones.

Kurzydlowski and Bucki [19] showed that, in the case of a bimodal Al polycrystal, the hardness could only be properly described by accounting for the dispersion about the mean GS, which, added to the mean GS, was used to uniquely define a lognormal grain size distribution. This higher-order microstructure description was also adopted by Berbenni *et al.* [25], who used a self-consistent scheme with a scale transition based on the translated fields to describe the effects of both the grain size distributions and the local heterogeneities on the mechanical response. As in the homogenization model of Weng [26], the crystal constitutive laws included a grain size effect using a Hall-Petch type dependence of the resolved shear stress. Several bimodal grain size distributions were compared, and a strong influence of the size ratio between the CG and UFG, and of the dispersion about the mean GS, on the yield stress was shown. This model was extended in Refs. [27, 28] by accounting for the different deformation mechanisms operating in the grain interior or in the vicinity of grain boundaries, which are related to statistically stored and geometrically necessary dislocations, respectively. Compared to the previous

work [25], hardening was well reproduced, but, as in Ref. [22], the thickness of the grain boundary dislocation pile up zone remained as an input parameter to the model. One may then resort to a calibration of this layer thickness from mesoscale field dislocation simulations [29], from lattice strain measurements using synchrotron diffraction [30] or from discrete dislocation dynamics [31].

A more direct modelling was later carried out by Magee and Ladani [32], using an explicit microstructure description and full-field simulations. The purpose was to examine the local deformation, the interaction between the two grain populations and the related failure mechanisms. To avoid prohibitive computation costs, the analyses were performed at two scales: *(i)* on the scale of a representative volume element (RVE) of the bimodal polycrystal, for which the microstructure corresponded to a homogeneous matrix of UFG with ellipsoidal inclusions of CG, each region being assigned an isotropic macro-homogeneous stress-strain behavior, and *(ii)* on a smaller scale, for which the interactions between the matrix of UFG and the CG were analysed using crystal plasticity and a cohesive interface model at the grain boundaries on the local scale of several UFG represented as a Voronoi tessellation. So, the interactions between UFG and CG were computed by accounting for the crystalline nature of the UFG population only. Although this enabled comprehensive analyses of the local mechanisms inside this population, its application was limited to the case of an UFG population in the form of diluted inclusions inside a CG homogeneous matrix.

In this work, a complete full-field modelling of polycrystals with an explicit high-resolution representation of the grains is presented. A large set of applications with such an approach were presented in [33, 34] and are extended here to constitutive modelling accounting for the effects of internal lengths. The article is organised as follows. In Section 2, we describe the microstructure generation process, constitutive behavior and identification of the material law parameters, and we determine the size of the RVE in a simplified case. In Section 3, we analyse a simple bimodal polycrystal with one CG, in terms of its macroscopic and local mechanical responses, for different crystallographic orientations of both CG and UFG. In Section 4, we analyse aggregates with multiple CG. In particular, crystal plasticity is compared to macro-homogeneous modelling, and the influence of CG spatial distributions on mechanical behavior is discussed. In Section 5, we close the article with conclusions.

For sake of simplicity in the following, the abbreviation FG will correspond equally to fine and ultrafine grains.

2. Numerical modelling

2.1. Microstructure generation

Microstructures are represented as Laguerre tessellations. A Laguerre tessellation of a domain of space, D, is defined from a set of seeds, S_i, of positions, x_i, and non-negative weights, w_i, $i \in [1, N]$. Each seed (S_i) is associated a Laguerre cell, C_i, as follows,

$$C_i = \left\{ P(x) \in D \mid d(P, S_i)^2 - w_i < d(P, S_j)^2 - w_j \ \ \forall j \neq i \right\} \tag{1}$$

The weight of a seed drives the size of its associated cell. The special case of Voronoi tessellation is obtained when all weights are equal. Compared to the widely-used Voronoi tessellations, Laguerre tessellations can include much higher contrasts of grain sizes [35], such as those found in bimodal polycrystals.

In this work, the seeds are generated following three successive steps:

1. Seeds corresponding to FG are arranged on a regular pattern (see Fig. 1a) and are assigned zero weights (w_i). The number of FG seeds is a function of the domain size and of the size of the FG. One or several seeds corresponding to CG are also added at controlled locations (see Fig. 1a). The FG seeds are assigned zero weights, and the CG seeds are assigned a weight equal to the target CG radius squared.
2. Seeds corresponding to FG are randomly perturbed about their original positions, by a random distance between 0 and the target FG radius, to latter generate random shapes (see Fig. 1b).
3. The FG seeds located within a CG radius of the CG seed(s) are removed (see Figs. 1c,d). (This step is optional and only aims at avoiding empty cells in the final tessellation.)

As will be seen in the following, this method offers great control on the grain sizes and the spatial distribution of the CG. The tessellation is then generated using Neper [36, 35]. A geometry regularization procedure is applied to remove small edges and faces (in 3D), which otherwise would be detrimental to mesh quality [36], and then the microstructure is meshed into 2nd-order triangular elements (in 2D) or tetrahedral elements (in 3D) [36]. A uniform element size is used, with typically 30 elements per FG. The mesh corresponding to the tessellation of Fig. 1 is provided on Fig. 2.

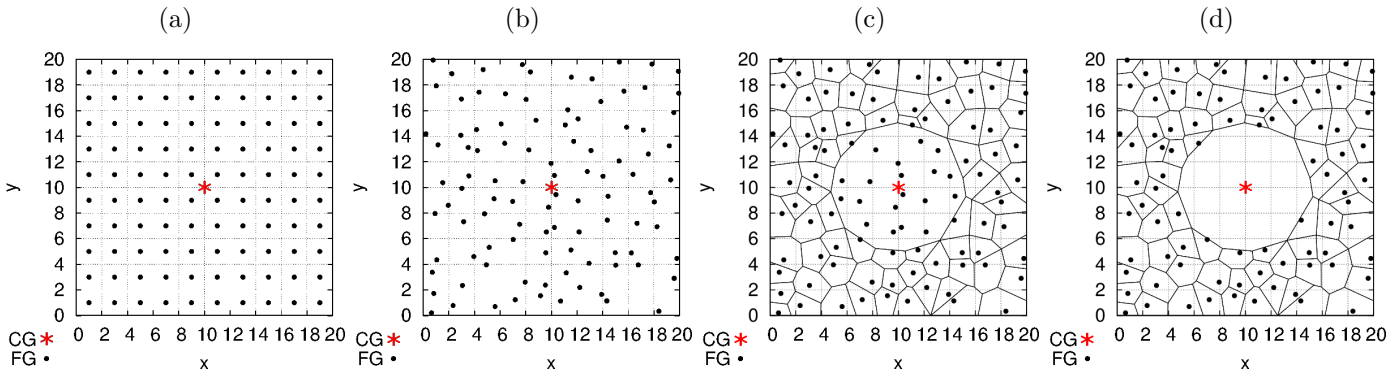

Figure 1: Generation of the seed distribution of a bimodal tessellation: (a) initial seed positions (regular pattern depending on the domain and grain sizes), (b) random perturbation about the initial positions, and (c) and (d) removal of the seeds surrounding the CG, for proper tessellation. On (c) and (d), the tessellation is plotted onto the seed distribution to better illustrate the seed generation process.

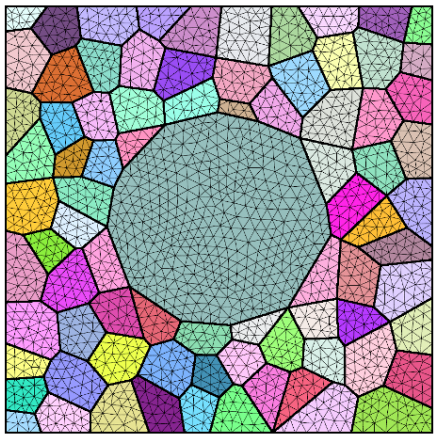

Figure 2: Mesh of the bimodal tessellation of Fig. 1. Note the high element quality, especially near grain boundaries and triple points, and the uniformity of the element size. The color mapping is only meant to distinguish the grains.

2.2. Crystal behavior

Elasticity is assumed isotropic, with values of Young modulus E and Poisson coefficient ν provided in Table 1. Plasticity operates by slip on the $\{1\,1\,1\}\langle 1\,1\,0\rangle$ systems. The slip rate of a given slip system, $\dot{\gamma}^s$, is related to its resolved shear stress, τ^s, through the Méric-Cailletaud formulation [1].

$$\dot{\gamma}^s = \left\langle \frac{|\tau^s - x^s| - r^s}{K} \right\rangle^n \operatorname{sign}(\tau^s - x^s), \tag{2}$$

where r_s is the isotropic hardening, x_s is the kinematic hardening, and K and n describe the Norton viscosity. In this work, as only monotonic tensile loadings are considered, kinematic hardening is discarded ($x^s = 0$).

A grain size effect will be introduced at the scale of individual slip systems by introducing a Hall-Petch type, size-dependent, hardening term in r^s. This is a simple but rather common approach [25, 37, 38], which is computationally-efficient and therefore applicable to the analysis of polycrystals with large numbers of grains. In contrast, approaches based on the mechanics of generalized continua, such as Cosserat, micromorphic or gradient-plasticity modellings [39, 40, 41, 42], introduce supplementary degrees of freedom and remain delicate to use with polycrystals with large numbers of grains.

The expression of the isotropic hardening, which includes a Hall-Petch-type grain size effect, is

$$\begin{aligned} r_g^s &= R_0^* + Q \sum_{u=1}^{12} h^{su} \left(1 - e^{-bp^u}\right) \\ R_0^* &= r_0^* + \frac{k^*}{\sqrt{d_g}} \end{aligned} \tag{3}$$

where R_0^* is the critical resolved shear stress, r_0^* is a critical resolved shear stress close to the one of a grain with a conventional grain size, k^* is a constant hardening parameter corresponding to the Hall-Petch slope on the scale of the slip system, and d_g is the size of the considered grain. d_g is defined as the diameter of the circle of equivalent area in 2D or sphere of equivalent volume in 3D. For the $\{1\,1\,1\}\langle 1\,1\,0\rangle$ systems considered here, h is a 12×12 matrix:

$$h = \begin{pmatrix} h_1 & h_2 & h_2 & h_4 & h_5 & h_5 & h_5 & h_6 & h_3 & h_5 & h_3 & h_6 \\ h_2 & h_1 & h_2 & h_5 & h_3 & h_6 & h_4 & h_5 & h_5 & h_5 & h_6 & h_3 \\ h_2 & h_2 & h_1 & h_5 & h_6 & h_3 & h_5 & h_3 & h_6 & h_4 & h_5 & h_5 \\ h_4 & h_5 & h_5 & h_1 & h_2 & h_2 & h_6 & h_5 & h_3 & h_6 & h_3 & h_5 \\ h_5 & h_3 & h_6 & h_2 & h_1 & h_2 & h_3 & h_5 & h_6 & h_5 & h_5 & h_4 \\ h_5 & h_6 & h_3 & h_2 & h_2 & h_1 & h_5 & h_4 & h_5 & h_3 & h_6 & h_5 \\ h_5 & h_4 & h_5 & h_6 & h_3 & h_5 & h_1 & h_2 & h_2 & h_6 & h_5 & h_3 \\ h_6 & h_5 & h_3 & h_5 & h_5 & h_4 & h_2 & h_1 & h_2 & h_3 & h_5 & h_6 \\ h_3 & h_5 & h_6 & h_3 & h_6 & h_5 & h_2 & h_2 & h_1 & h_5 & h_4 & h_5 \\ h_5 & h_5 & h_4 & h_6 & h_5 & h_3 & h_6 & h_3 & h_5 & h_1 & h_2 & h_2 \\ h_3 & h_6 & h_5 & h_3 & h_5 & h_6 & h_5 & h_5 & h_4 & h_2 & h_1 & h_2 \\ h_6 & h_3 & h_5 & h_5 & h_4 & h_5 & h_3 & h_6 & h_5 & h_2 & h_2 & h_1 \end{pmatrix}, \tag{4}$$

which, due to symmetry considerations, contains only six independent parameters [43]. The diagonal terms, which are equal to h_1, represent self hardening. Non-diagonal terms, $h_{2\text{–}6}$, represent latent hardenings of different types: coplanar interactions, Hirth locks, cross slip interactions, glissile junctions and Lomer-Cottrel locks, respectively. As explained in [44], the respective influence of interactions and the order of the hardening coefficients can be contradictory according to the means to address these questions (experimental or numerical analyses) and are shown to differ if the crystal plasticity model is based on dislocation densities or on a local phenomenological hardening on the scale of the slip systems. In this study, the retained values are taken from [1] which were concerning copper and were based on the Méric-Cailletaud model.

2.3. Identification of material parameters

The material parameters appearing in Eqs. 2 and 3 can be classified in two families. The first family contains the parameters not involved in the GS dependence: K, n, Q, h and b. Among them, K, n and h are set to typical values (summarized in Table 1), while Q and b will be identified from the stress-strain curve of a material with a conventional (i.e., relatively large) GS. The second family contains the parameters involved in the GS dependence: r_0^* and k^*. They can be identified from the stress-strain curves obtained from a same material at different average GSs (all other parameters being unchanged).

All the simulations for the identification procedure have been carried out on a 3D polycrystal containing 125 equiaxed grains with random crystal orientations (fig. 3 and 4). For each simulation, the size of the polycrystal was set according to the considered experimental reference and a simple tensile test was performed with imposed longitudinal displacements and stress-free lateral faces.

2.3.1. Identification of Q and b

The experimental stress-strain curve of a specimen of fully recrystallised 316L stainless steel with an average GS of about 50 µm is used. From a simulation to the other, Q and b have been adjusted to minimize the difference between the experimental and simulated stress-strain curves, which are represented on Fig. 3. Table 1 provides the corresponding values of Q and b.

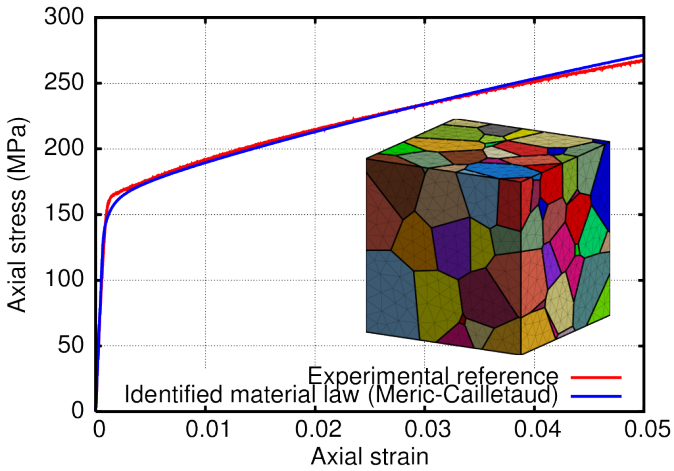

Figure 3: Identification of parameters Q and b from the stress-strain curve of a material with a conventional grain size ($d_g = 50$ µm). The 125-grain polycrystal used for simulations is also represented. Note the good match between the experimental and simulated curves.

2.3.2. Identification of r_0^* and k^*

The identification of these parameters is based on the reference experimental characterization of the Hall-Petch effect in a 316L stainless steel [7]. This experimental characterization provides the values of σ_0 and k describing the macroscopic Hall-Petch effect on the yield stress σ_y:

$$\sigma_y = \sigma_0 + \frac{k}{\sqrt{d_g}} \tag{5}$$

r_0^* is assumed to be related to σ_0 through the average Taylor factor of the grains, $\langle M \rangle$,

$$r_0^* = \frac{\sigma_0}{\langle M \rangle} \tag{6}$$

Following [7], we use $\sigma_0 = 105$ MPa, $k = 1000$ MPa.μm$^{-1/2}$ and, considering a random distribution of crystal orientations as in the experimental sample, $\langle M \rangle = 3.06$, which finally yields $r_0^* = 34.3$ MPa.

The Hall-Petch slope k^* on the slip system scale is determined from the evolution of the yield stress as a function of grain size. To do this, a simple scaling is applied on the numerical polycrystal such as to vary its average GS. Four sizes are considered: $d_g = 55$ µm, 40 µm, 15 µm and 2 µm. Fig. 4a,b show the polycrystals and the corresponding stress-strain curves, respectively. From the stress-strain curves, the yield stresses are determined at 0.2% plastic deformation and then reported on a Hall-Petch plot of the macroscopic response such as seen on Fig. 4c. One may note that the introduction of the Hall-Petch term on the scale of the slip system leads to the Hall-Petch effect on the macroscopic scale. The appropriated k^* is identified as the one which enables to obtain the reference macroscopic slope k taken from Ref. [7]. The value is provided in Table 1.

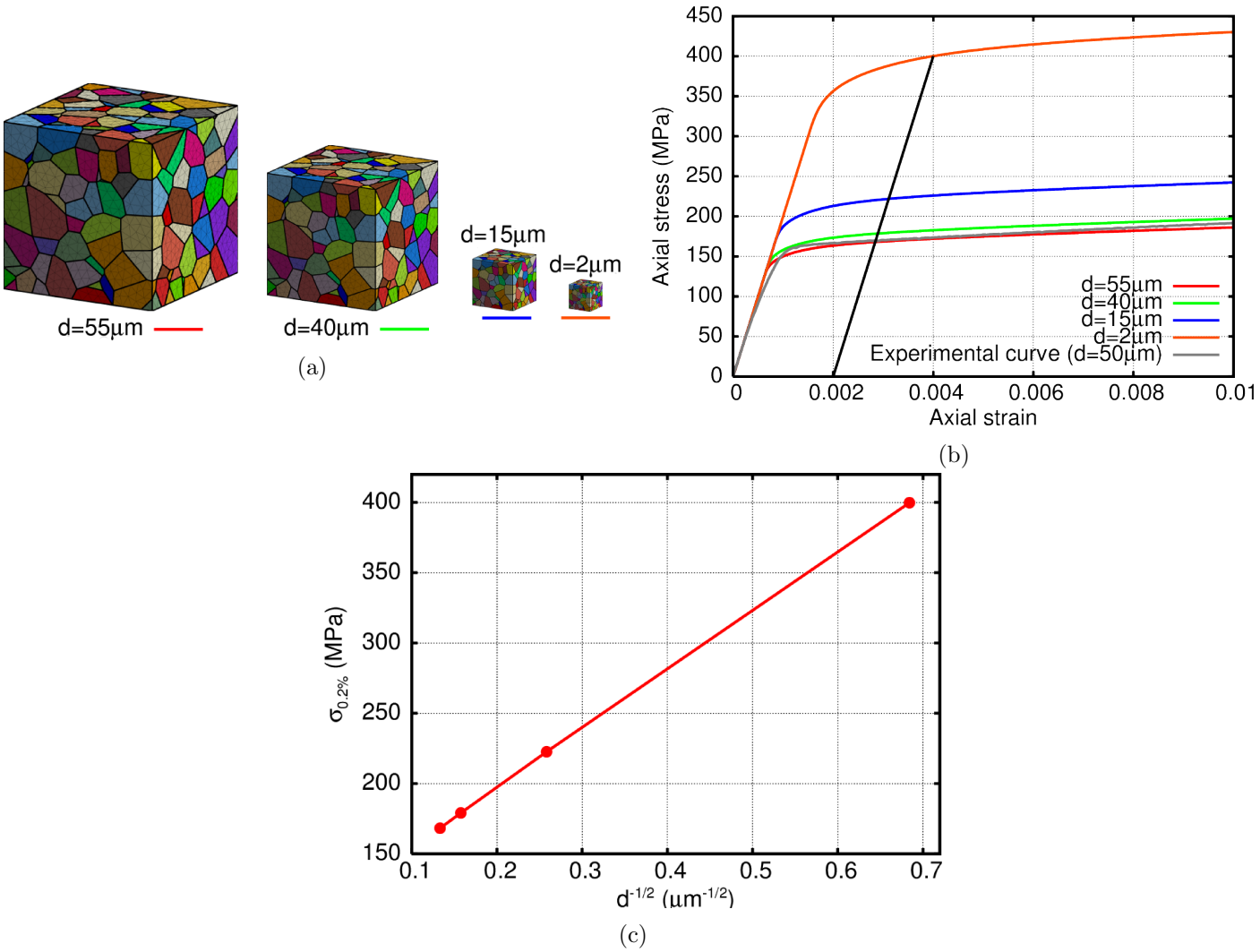

Figure 4: Identification of parameters r_0^* and k^*. (a) 125-grain polycrystals of different grain sizes, (b) corresponding stress-strain curves and yield stress ($\sigma_{0.2\%}$) determination, and (c) Hall-Petch plot on the macroscopic scale of the polycrystals, obtained with a given k^*. The slope of the numerical Hall-Petch plot in (c) is compared to the macroscopic experimental one (k in Eq. 5) in order to identify k^*.

Table 1: Material parameters used in the finite element simulations. h^{su} values after [1].

Elasticity		Plasticity, no GS dependence								Plasticity, GS dependence	
E (GPa)	ν	Q (MPa)	b	K (MPa.s$^{1/n}$)	n	h_1	h_2	h_{3-5}	h_6	r_0^* (MPa)	k^* (MPa.µm$^{-1/2}$)
200	0.3	10	9.06	9	24	1.00	4.40	4.75	5.00	34.3	200

3. Bimodal polycrystal with one coarse grain

This section considers the case of a bimodal polycrystal with a single central CG, in 2D and 3D. The aim is to investigate first the influence of the boundary conditions, especially in 2D case, on the effective properties of a polycrystal (Section 3.1), and then the influence of the FG and CG crystallographic orientations on both the effective properties of the polycrystal and the local mechanical fields (Section 3.2). A tensile deformation of 1% is considered. Focus is drawn on the strain and stress fields at 1% strain, and on the yield stress.

3.1. Comparison of 2D and 3D polycrystals, and influence of boundary conditions

Given the large grain size ratio between the CG and FG that will be used in the following (5 and 10), large numbers of grains will be necessary in the simulations, especially when several CG are used. It then becomes desirable to use 2D-extruded polycrystals instead of 3D polycrystals. The behaviour should remain essentially unchanged, however, which can be verified as follows.

A 3D unimodal polycrystal with 7^3 (343) grains is used as a reference. This number of grains is considered sufficiently large to get representative results; in other words, the polycrystal can be considered as a representative volume element (RVE). Displacements are imposed on the two opposite z surfaces (while other surfaces are free), as can be seen on Fig. 5a, and which is similar to experimental conditions.

A "2D-extruded" polycrystal with the same linear density of grains (number of grains along a dimension) as the 3D polycrystal is then used. The polycrystal is essentially 2D, but it is extruded in the third direction by the length of one element. Such a 2D configuration raises the question of what should be the boundary conditions along the extrusion direction. Here, we will determine the conditions such that the macroscopic behaviour of the 2D polycrystal is as close as possible to the one of the 3D polycrystal.

While the "standard" faces of the 2D-extruded specimen (in directions y and z, on Fig. 5b) are applied the same conditions as for the 3D polycrystal (free conditions and imposed displacements, respectively), the faces along the extrusion directions can be applied different conditions:

- zero forces (plane stress);
- zero displacement (plane strain);
- faces remain flat and parallel to themselves.

The two first solutions are extremes, and the third one provides mixed conditions, as a Poisson effect along the extrusion direction is enabled but is set to remain uniform: in this extrusion direction, all grains undergo the same average deformation, irrespective of their sizes, locations and crystal orientations. This solution can also be seen as a way to account for an average contribution of the grains that would be present along the extrusion direction, should the polycrystal be 3D. Figures 6a and 6b show the stress-strain curves for the cases described previously, and for two numbers of grains (along a direction) for the 2D-extruded polycrystal: 7 and 14, respectively. Both figures show the same trends: a 2D-extruded polycrystal with plane stress conditions does not exhibit significant hardening, likely due to early, extended strain localisation, while a 2D-extruded polycrystal with plane strain conditions exhibits similar hardening but a higher stiffness than a 3D polycrystal. As expected, the behaviour of the 2D-extruded polycrystal with flat and parallel faces lies between those of the two previous (and extreme) cases: compared to the 3D polycrystal, the yield stress is slightly underestimated but the hardening is close. This case will be used consistently in the following.

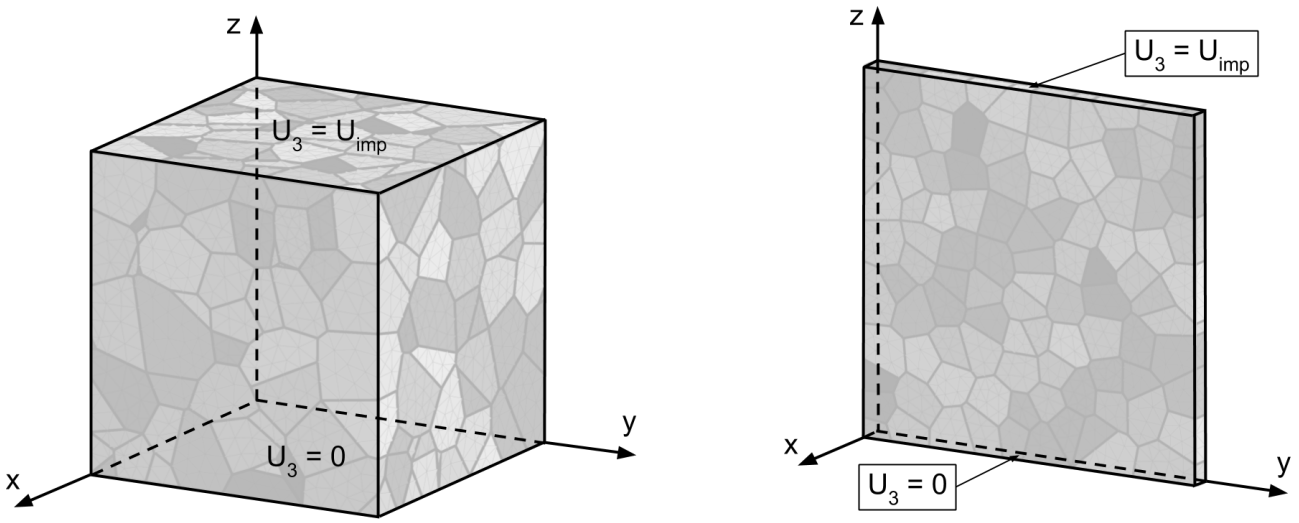

(a) (b)

Figure 5: Boundary conditions on (a) 3D and (b) 2D-extruded polycrystals.

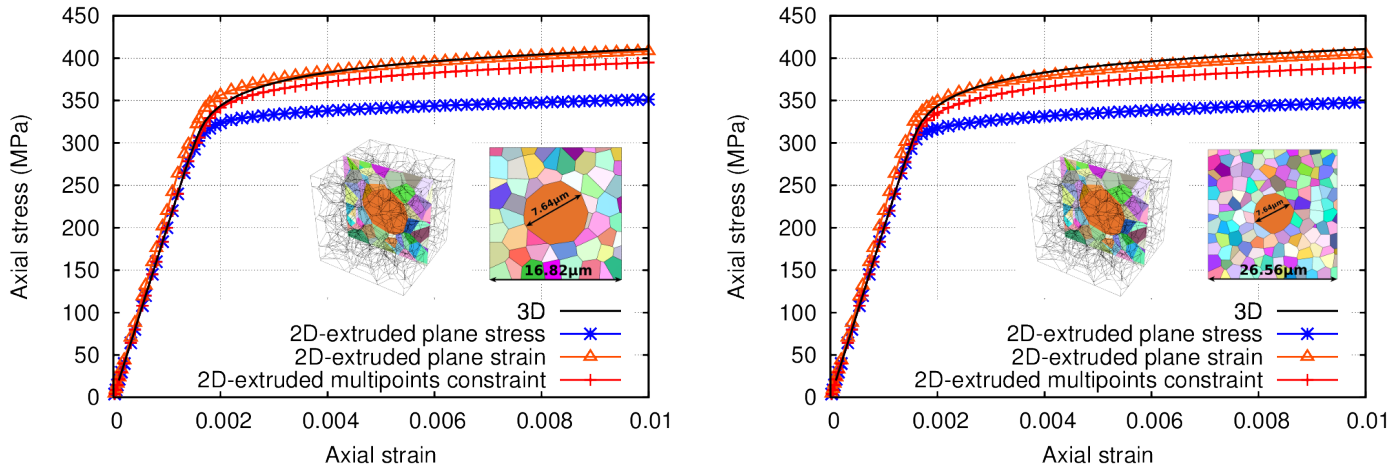

(a) (b)

Figure 6: Comparison of macroscopic stress-strain curves for 3D and 2D-extruded polycrystals with different boundary conditions on the extrusion faces. Two microstructures are used to ensure that results do not depend on the number of FG: (a) and (b) polycrystals contain respectively about 7 and 14 FG along the y and z directions.

3.2. Influence of the CG and FG orientations

The influence of the crystal orientations of the grains on the global and local behaviour of the polycrystal is analysed by considering two different orientations of the CG: [0 0 1] ∥ tensile direction (8 potential active slip systems) and [1 2 3] ∥ tensile direction (1 favourable slip system), and two sets of (random) orientations for the surrounding FG.

Figure 7 provides the computed stress-strain curves of the polycrystal for the different orientation configurations. It can be seen that the crystal orientations of both CG and FG have a small influence on the effective mechanical properties of a bimodal polycrystal with a single central CG, which tends to confirm that the polycrystal is close to a RVE.

Figures 8 and 9 provide the strain and stress fields inside polycrystals, respectively, as well as line profiles and grain-averaged values along these profiles. These figures provide information for the understanding of the influence of the CG and FG-matrix orientations on the local fields. First, the strain tends to localise as bands oriented at 45° with respect to the tensile direction (the direction of maximal macroscopic shear), a common observation [45]. Second, similar strain localisation patterns are observed for the two CG orientations (and fixed FG-matrix orientations); only the strain levels are slightly modified (Figs. 8a and 8b). At the opposite, different FG orientations (Figs. 8a vs 8c) modify both the strain localisation pattern and strain intensities. Finally, the CG and FG orientations have only a limited effect on stress fields. Stresses are slightly higher with CG of [1 2 3] orientation than with [0 0 1] orientation (Fig. 9b), which could be explained by the fact that only one system is favourably oriented for slip in the [1 2 3] CG. The stress pattern remains essentially unchanged, however, with softening on both sides of the CG along the tensile direction, and stress concentration in FG, at the interface with the CG along the transverse direction. This stress concentration is especially visible on the line profiles for the three polycrystals (Figs. 9d, 9e and 9f).

Figures 8g,h,i and 9g,h,i show the probability density functions (PDF) of, respectively, the axial strain and stress, for the same polycrystals as in Fig. 7, and at a macroscopic strain of 1%. These PDF are computed from the strain and stress values at each integration point of the mesh. They confirm the GS dependence from the statistical point of view, for the three polycrystal configurations: the CG develops the highest strains while FG supports the highest stresses. It is also seen that the [1 2 3] CG undergoes the smallest strains and leads to a sharpening of the stress distribution by comparison to the [0 0 1] case. This once again can be related to the less number of favourably oriented slip systems in the [1 2 3] CG. In summary, whereas the nature of the FG matrix plays the major role on the strain localisation patterns, the orientation of the CG is the main factor impacting the statistical broadening of the intragranular stresses and strains.

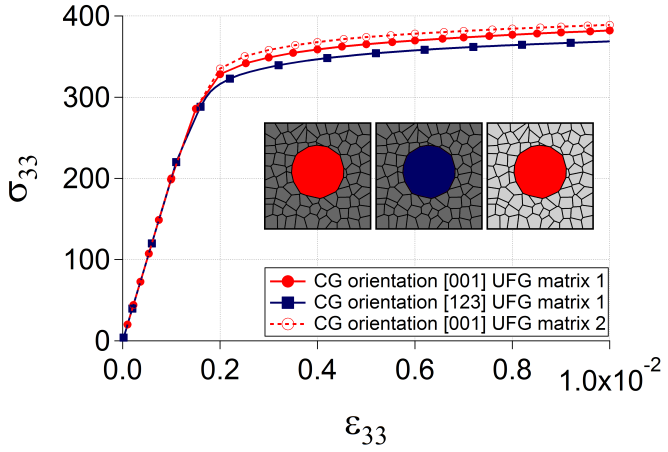

Figure 7: Stress-strain curves for a bimodal polycrystal with one central CG and different CG and FG orientations. The polycrystal contains 85 grains.

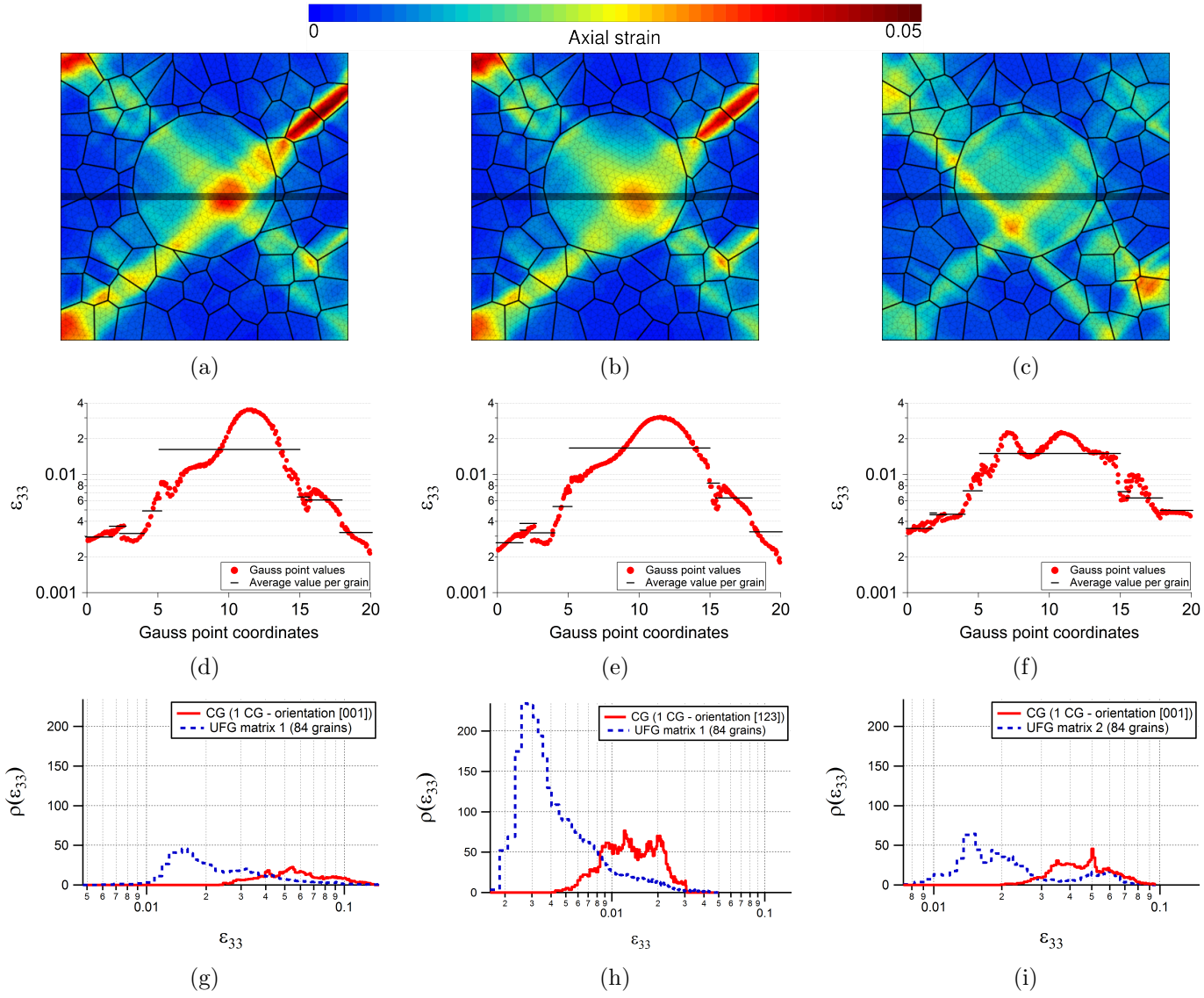

Figure 8: Strain fields for bimodal polycrystals containing one central CG, and of the same grain shapes but different grain orientations. (a) CG orientation [0 0 1] and FG matrix 1, (b) CG orientation [1 2 3] and FG matrix 1, and (c) CG orientation [0 0 1] and FG matrix 2. (d–f) Corresponding strain profiles and grain-averaged values. The line profile is shown by a gray line on (a–c). (g–i) Corresponding strain probability density functions. The polycrystal contains 85 grains and is deformed to 1%. The tensile direction is vertical.

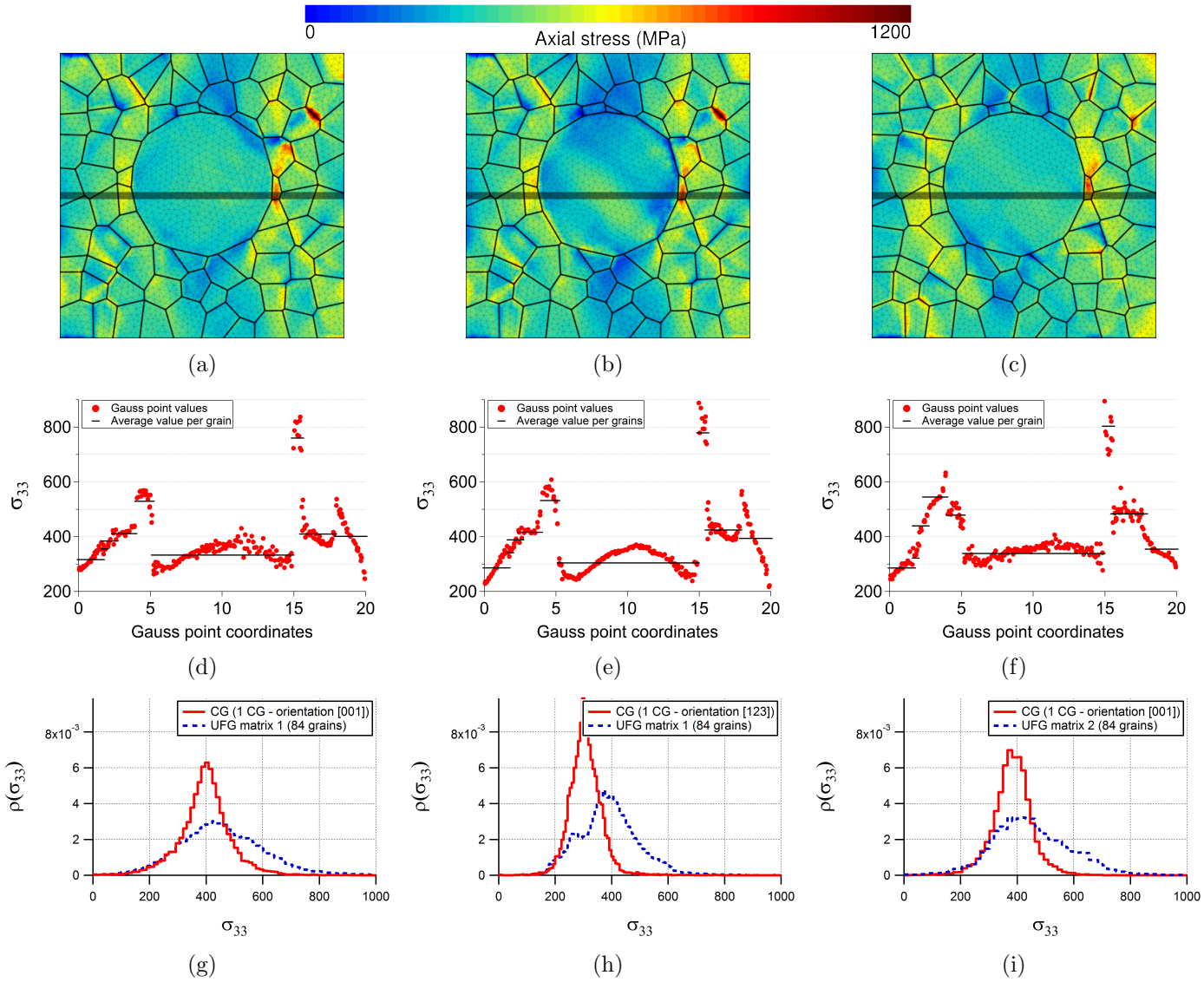

Figure 9: Stress fields for bimodal polycrystals containing one central CG, and of the same grain shapes but different grain orientations. (a) CG orientation [0 0 1] and FG matrix 1, (b) CG orientation [1 2 3] and FG matrix 1, and (c) CG orientation [0 0 1] and FG matrix 2. (d–f) Corresponding strain profiles and grain-averaged values. The line profile is shown by a gray line on (a–c). (g–i) Corresponding stress probability density functions. The polycrystal contains 85 grains and is deformed to 1%. The tensile direction is vertical.

4. Bimodal polycrystals with multiple coarse grains

This section considers the case of bimodal polycrystals with multiple CG. The aim is to investigate first the influence of the number of CG and to define the size of the RVE in the ranges of GS and GS ratios considered in this study (Section 4.1), then the difference between our full-field crystal plasticity modelling and macrohomogeneous modellings (Section 4.2), and finally the influence of grain size distributions and CG spatial distributions on macroscopic and local mechanical responses (Section 4.3). As in Section 3, a tensile deformation of 1% is considered.

4.1. Size of the representative volume element

In previous works [46, 47, 42], it was shown numerically or experimentally that, for unimodal grain size distribution and equiaxed grains, a minimum of seven grains along each direction of the polycrystal should be considered to avoid free surfaces effect (*e.g.*, like in thin films). It is here necessary to renew the analysis in the case of a bimodal polycrystal, to determine what would be the minimum number of CG (for a 2D polycrystal). The objective is to determine the size of the RVE to a first order, i.e. considering only the effective properties. To this purpose, the simplified case of CG regularly distributed in a matrix of FG is considered.

The procedure is to consider polycrystals of increasing numbers of CG, and to determine their yield stresses. The CG are arranged on square arrays of 1×1 up to 5×5 CG. As before, two CG orientations are considered: the high-symmetry [0 0 1] orientation and the non-symmetrical [1 2 3] orientation. For the [0 0 1] orientation, eight slip systems are expected to be simultaneously activated upon yielding, while for the [1 2 3] orientation, one slip system is more favourably oriented than others. As for the FG, orientations are random. Figure 10 provides the evolution of the yield stress as a function of the number of CG, and a convergence of σ_y is seen at about 9 CG. A number of 9 CG in the polycrystal therefore provides the best compromise between accuracy and computation cost.

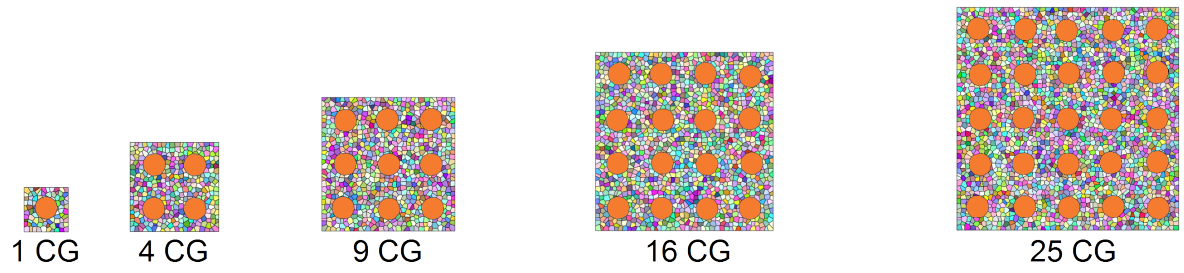

(a)

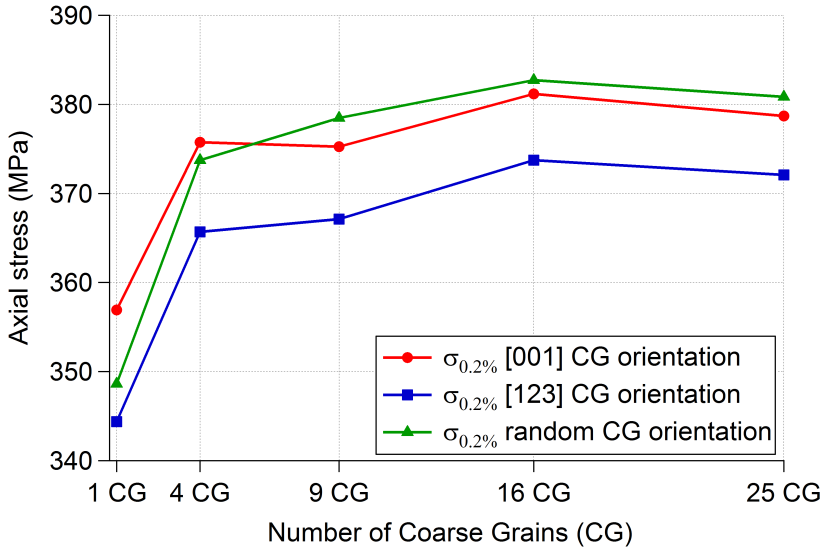

(b)

Figure 10: Determination of the size of the RVE. (a) Polycrystals with 1×1 up to 5×5 CG and (b) yield stress as a function of the number of CG, for different crystal orientations.

4.2. Comparison of crystal plasticity and macro-homogeneous modellings

As pointed out in Section 1, some of the models of bimodal polycrystals presented in the literature assume that CG and FG are homogeneous phases, as in an inclusion-matrix composite. In the latter case, this type of modelling was very successful to predict not only effective properties but also the tortuosity of the strain localisation patterns (see e.g. [48]). In this section, we will compare modellings based on macro-homogeneous (MH) and crystal plasticity (CP) behaviors, as illustrated on Fig. 11. As before, focus will be drawn on both macroscopic and local responses.

For the MH modelling, each phase is assigned an elastoplastic isotropic and homogeneous behavior with a non-linear isotropic hardening. The parameters of a given MH phase (corresponding to a given average GS) have been identified from the macroscopic stress-strain curve of the 125-grain unimodal polycrystal of section 2.3.2 with the appropriate average GS.

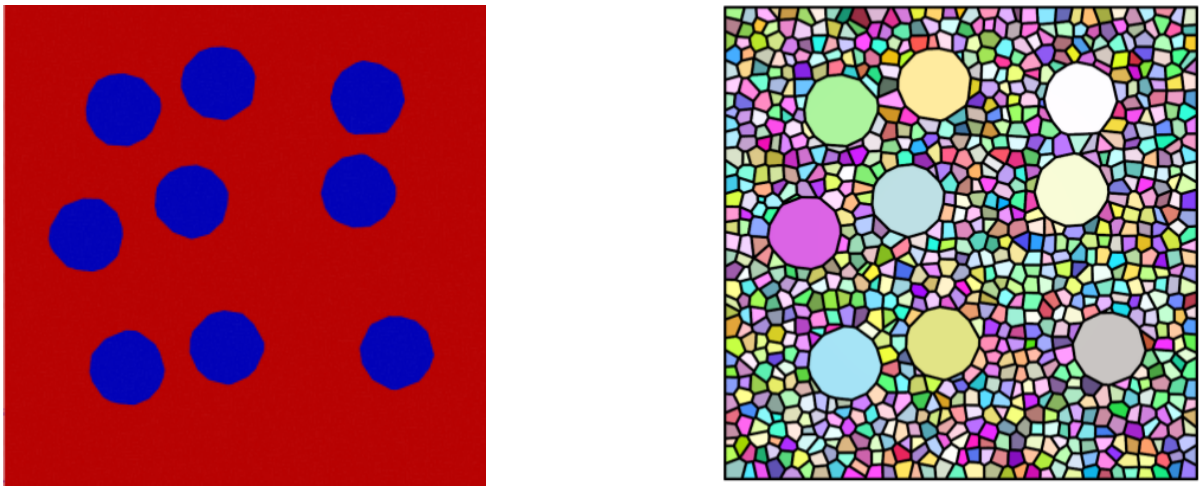

(a) (b)

Figure 11: Modellings based on (a) macro-homogeneous phases and (b) crystal plasticity, for the same polycrystal. In (a), FG are represented by the red matrix, and CG are represented in blue. In (b), grains are coloured according to their orientations.

4.2.1. Macroscopic scale

Bimodal polycrystals of different grain sizes, grain size ratios between the two populations and spatial distributions of coarse grains are considered. Fig. 12 provides their yield stresses, as obtained by MH or CP modellings. For each FG-CG couple, the Voigt (upper) bound is also provided. It is obtained by the linear rule of mixture of the yield stresses of the two grain populations.

MH and CP modellings provide similar yield stresses for small GS ratios and small CG volume fractions, but significant differences appear, as the GS ratio and CG volume fraction increase. This effect is likely to be related to more intense CG clustering, and to the spatial distribution of CG, for the highest CG volume fractions. At the opposite, a configuration with isolated CG is similar to the diluted scheme of a classical homogenisation problem, for which the Voigt bound appears as a good first-order approximation.

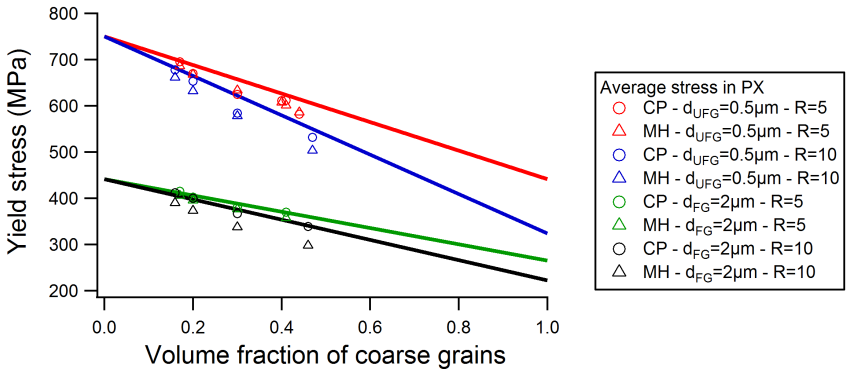

Figure 12: Yield stress of bimodal polycrystal of different grain sizes and volume fractions. Voigt upper bounds are provided as solid lines. CP: crystal plasticity modelling, MH: macro-homogeneous modelling.

4.2.2. Intragranular scale

The strain and stress fields developing in a bimodal polycrystal with CG of 2.5 µm and FG of 0.5 µm (grain size ratio of 5), as obtained by the MH and CP modellings, are presented in Fig. 13.
While the yield stress does not vary much, the local fields predicted by the two modelling types are significantly different. It is therefore necessary to take into account the polycrystalline nature of the material for accurate modelling at a local scale. Only CP modelling produces the features typically encountered in deformed polycrystals, such as intense strain localisation bands [45, 49]. In a similar way, CP modelling provides stress heterogeneities very different to those obtains by MH modelling. Namely, while MH modelling predicts stress concentrations only about CG (in the horizontal direction), CP modelling predicts much higher heterogeneity, especially at the small scale of FG.

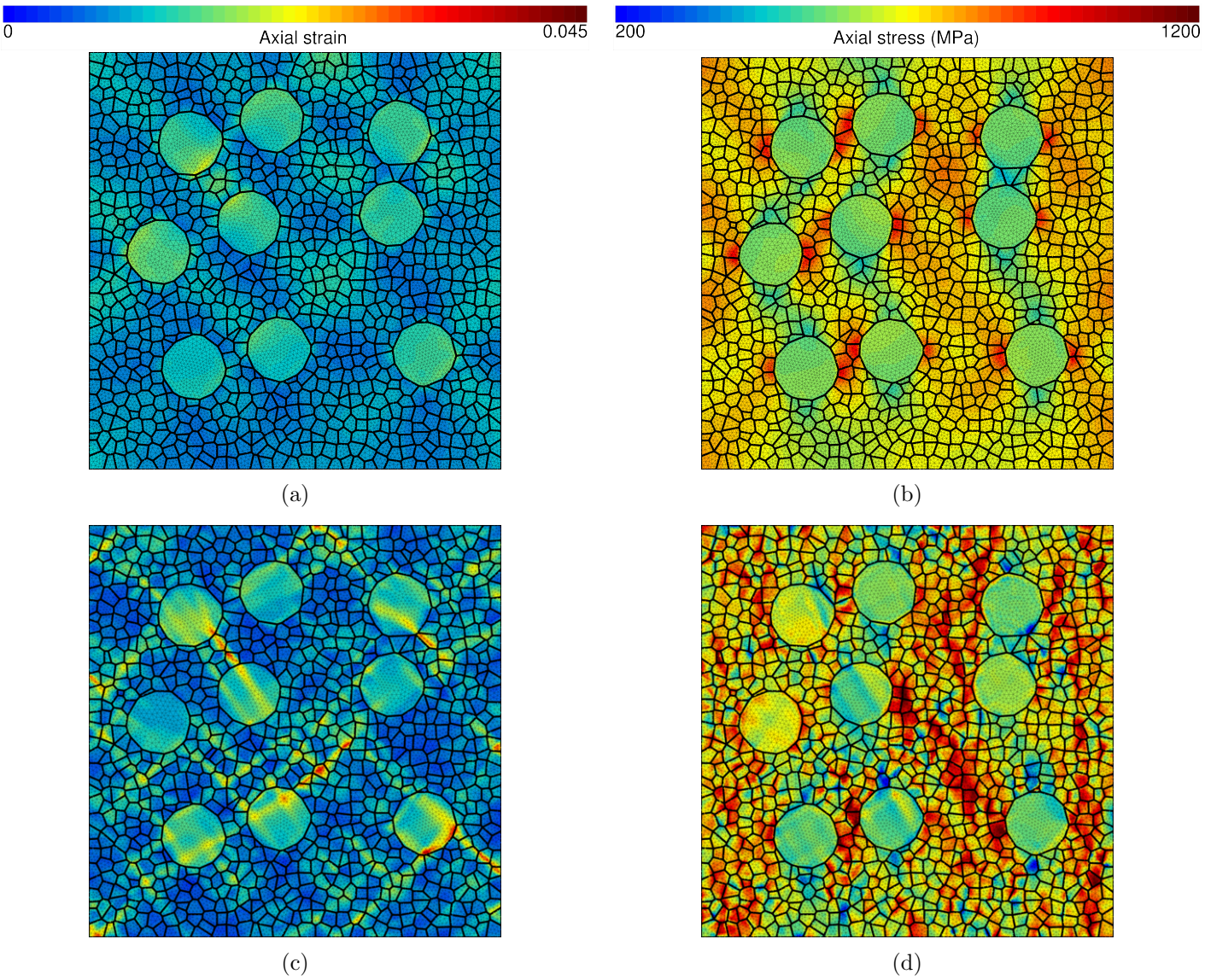

Figure 13: Stress and strain fields in a bimodal polycrystal, as predicted by macro-homogeneous or crystal plasticity modellings. (a, c) strain and (b, d) stress. (a, b) macro-homogeneous modelling and (c,d) crystal plasticity modelling. The tensile direction is vertical.

4.3. Influence of the CG spatial distribution

The influence of the CG spatial distribution is analysed systematically, for four sets of CG and FG sizes taken from previous experimental works [20] and listed in Table 2. For each set, three different CG spatial distributions are considered:

- "Clusters": CG forming clusters, as shown on Figs. 14a and 14d (CG volume fraction of about 30%),
- "Groups": CG (potentially) in contact but not forming clusters, as shown on Figs. 14b and 14e (CG volume fraction of about 20%),
- "Isolated": CG not being in contact (and so, not forming clusters), as shown on Figs. 14c and 14f (CG volume fraction of about 17%),

which results in 12 different microstructures. The (six) microstructures with FG size equal to 0.5 µm are represented on Fig. 14.

Table 2: FG and CG grain sizes of the bimodal polycrystals considered to analyse the influence of the CG spatial distribution.

FG grain size (µm)	0.5	0.5	2	2
CG grain size (µm)	2.5	5	10	20
CG/FG grain size ratio	5	10	5	10

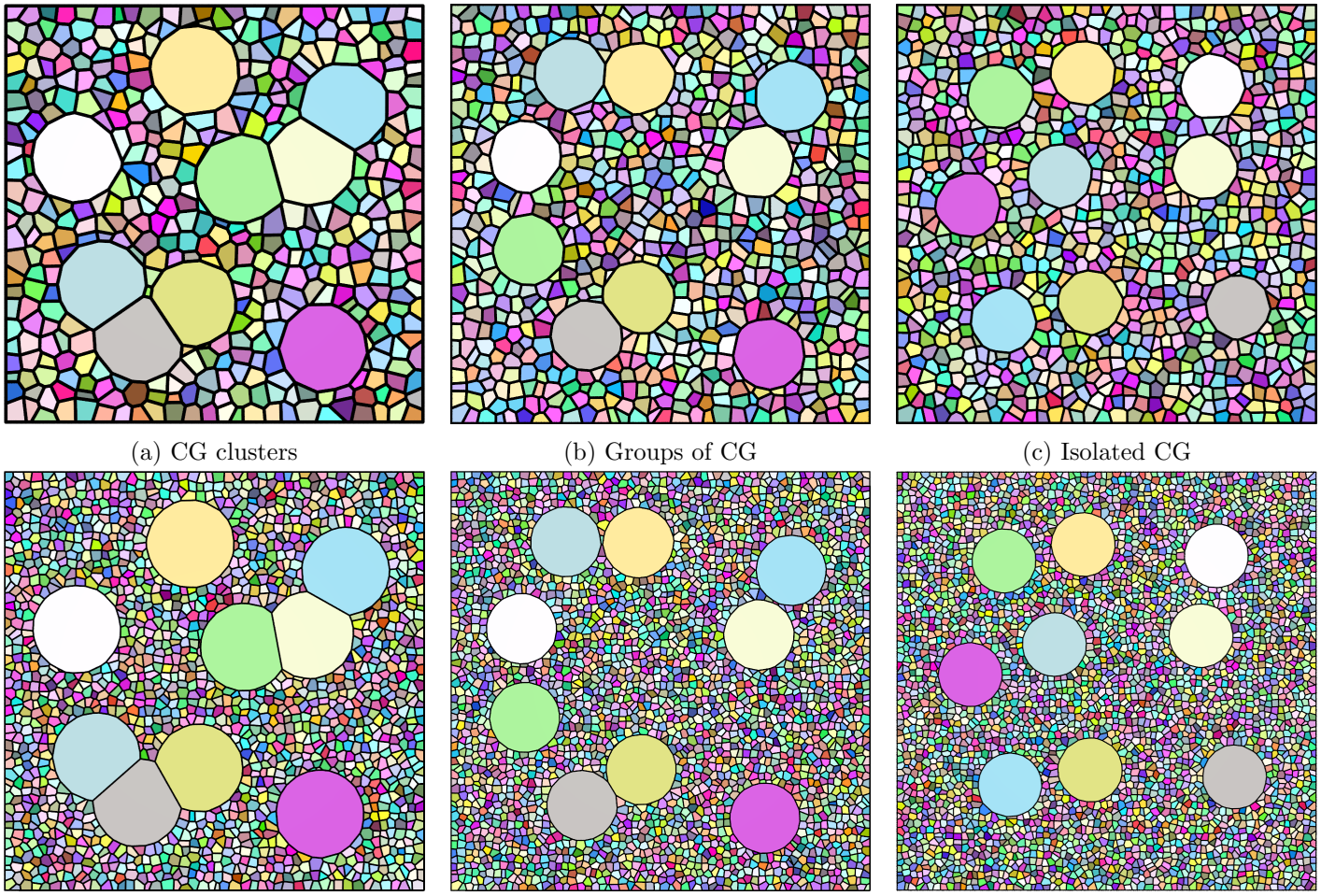

(a) CG clusters (b) Groups of CG (c) Isolated CG

(d) CG clusters (e) Groups of CG (f) Isolated CG

Figure 14: Microstructures considered to analyse the influence of the CG distribution. (a–c) Grain size ratio of 5 and (d–f) grain size ratio of 10. The size of FG is about 0.5 µm.

Fig. 15 provides the stress-strain curves of all polycrystals. Two experimental curves corresponding to approximately the same average grain sizes of CG and FG and to 25% of CG in volume fraction are also represented [20]. As seen from the numerical results alone, the spatial distribution of CG plays a role only for the smallest size of FG (0.5 µm), and this effect increases with the grain size ratio. As compared to the experimental curves, the modelling provides a correct prediction in any case of CG spatial distribution for a FG size of 2 µm. But for FG of 0.5 µm, only the case of clustered CG fits the experimental curve, where clusters of CG were also present. This shows that isolated or clustered CG configurations should be differentiated in the process of microstructure-based modeling.

In order to dissociate CG volume fraction effect from CG morphology effect from a quantitative point of view, it is proposed to take the Voigt (upper) bound of the yield stress as a reference yield stress (YS) for each considered volume fraction of CG and to normalize the crystal plasticity YS by these reference YS. As represented on Fig. 16, the YS can be approximated by the Voigt YS with an error of 5% if CG are isolated. But if CG are clustered, then the difference reaches from 10 to 15%, which confirms the necessity to account explicitely for the spatial arrangement of CG.

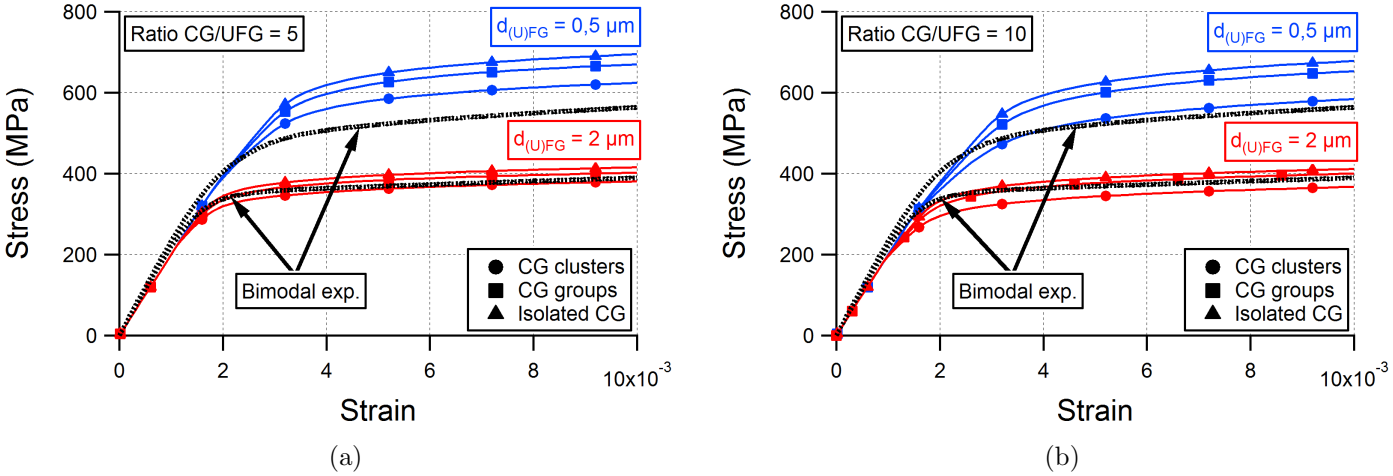

Figure 15: Influence of the CG distribution on macroscopic mechanical responses: (a) grain size ratio of 5 and (b) grain size ratio of 10.

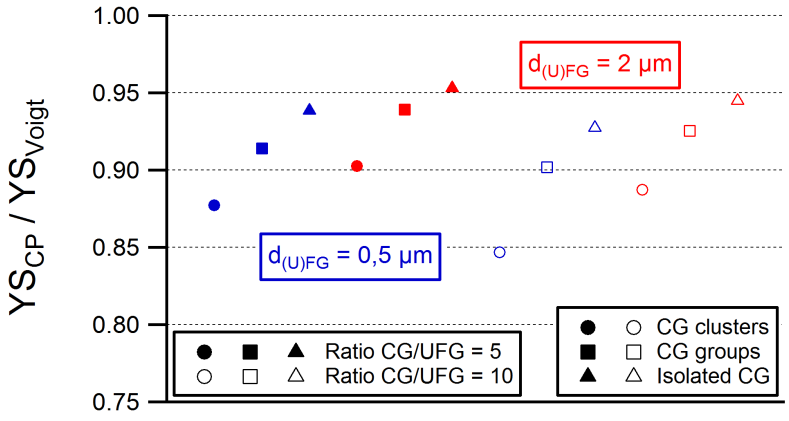

Figure 16: Crystal plasticity yield stresses (at 0.2% plastic deformation offset) normalized by their corresponding Voigt upper bound yield stresses.

The strain and stress fields of the polycrystals of Fig. 14 are provided on Figs. 17 and 18, respectively.

Whatever the considered microstructure and GS ratio, the strain and stress fields show localisation patterns which are commonly observed in polycrystals, irrespective of their GS distribution: 45°-oriented strain localisation bands and a high stress heterogeneity from grain to grain [45]. Bimodal polycrystals differ from unimodal ones by three main features, which were also observed in the case of a single CG: *(i)* strain localisation bands which appear particularly intense and sometimes extend over the whole polycrystal because of the presence of CG, *(ii)* high stresses which concentrate in FG at the vicinity of CG and along the transverse direction and *(iii)*, consistently, low stress channels above and below CG which expand over several FG along the tensile direction. These three characteristics of the stress and strain fields were also observed in the matrix-inclusion composite modelling with macro-homogeneous constitutive laws, but as seen in fig. 13, the intensity of localisation is considerably underestimated as compared to crystal plasticity modelling. There is no significant effect of the GS ratio on these characteristicsi, but grain clustering does lead to two main effects: it favours the intensification and the extension of strain localisation bands, and it promotes the widening (along the transverse direction) of the relaxation channels.

These observations are corroborated, from a statistical point of view, by comparing the mean responses per grain at 1% imposed axial strain in the cases of isolated or clustered CG, as presented in Fig. 19. It is indeed observed that, from the isolated to the clustered case, a higher dispersion of strain towards both smaller and larger values is obtained, an effect which may be related to grains in the characteristic localisation regions (*viz.* strain localisation bands and relaxation channels). Although clusters can be suspected from field contour plots to promote stress concentration in the vicinity of the FG/CG interfaces, the analysis on the distribution of mean stress per grain shows that there is no significant effect of the CG clusters on the dispersion of stresses. On the contrary, CG clusters lead to stress and strain distributions whose peaks are shifted to slightly smaller values than in the isolated case and, moreover, they reduce the mean stress and strain of the FG population by approximately 15%.

These results show that not only the grain sizes but also the CG spatial distribution affect the mechanical response of bimodal polycrystals, at both local and global scales. The CG are observed to increase stresses along the transverse direction and to decrease them along the longitudinal direction, in both cases by a factor of $2-3$ (as measured from the stress fields) with respect to the mean polycrystal stress. However whereas the stress increase remains confined to a few grains close to the FG/CG interface, the stress relaxation develops along large and long longitudinal channels. This ability of the CG to accomodate the stresses of FG on a relatively long range along the tensile direction comes in agreement with our observations in the related experimental study [20]: a ductility improvement was obtained by introducing CG clusters in the FG material and this was correlated to a relaxation of the (long range interaction) backstress.

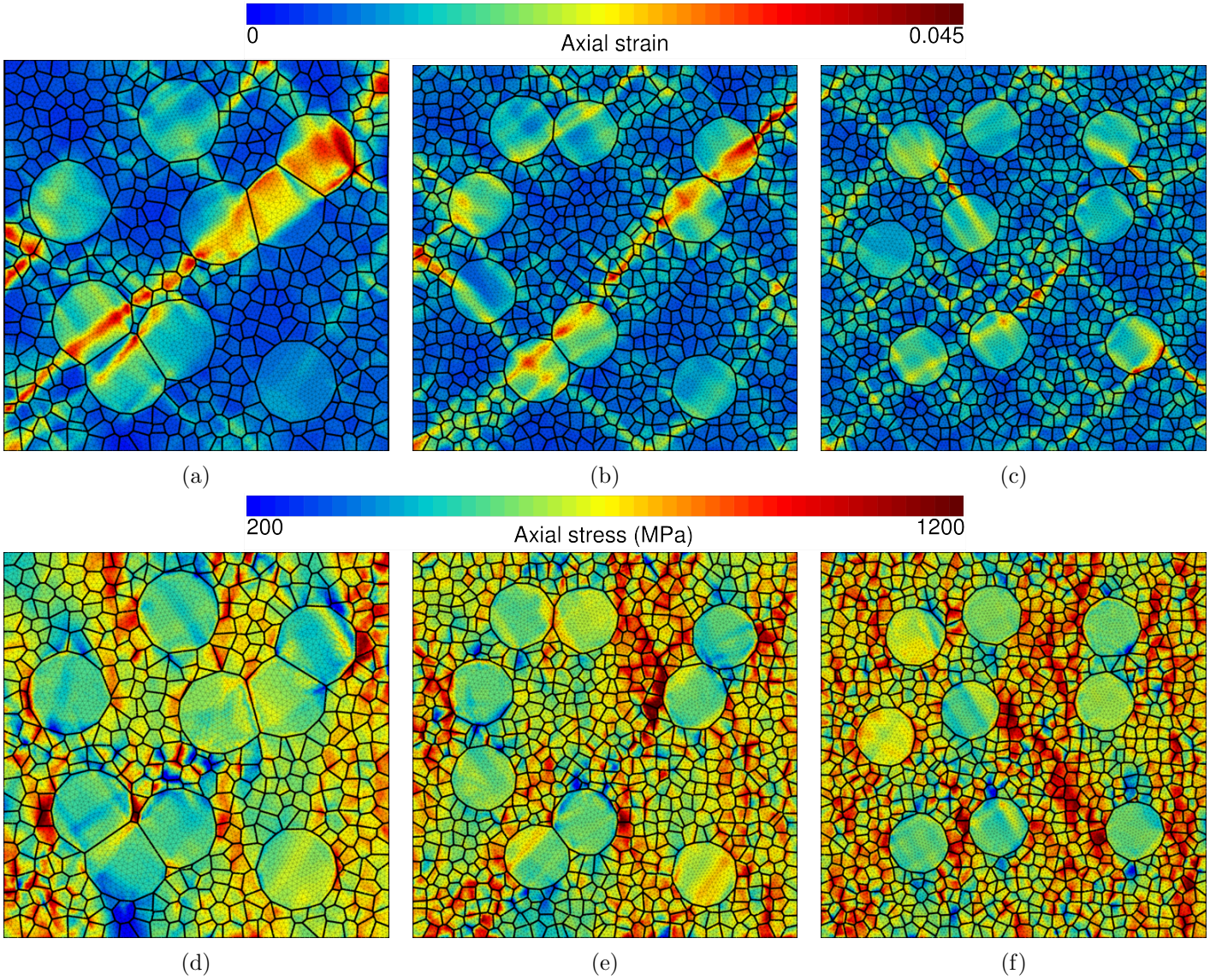

Figure 17: Influence of the CG distribution on the strain and stress fields for a grain size ratio of 5: (a, d) Clusters, (b, e) Groups and (c, f) Isolated. The size of FG is about 0.5 µm. The tensile direction is vertical.

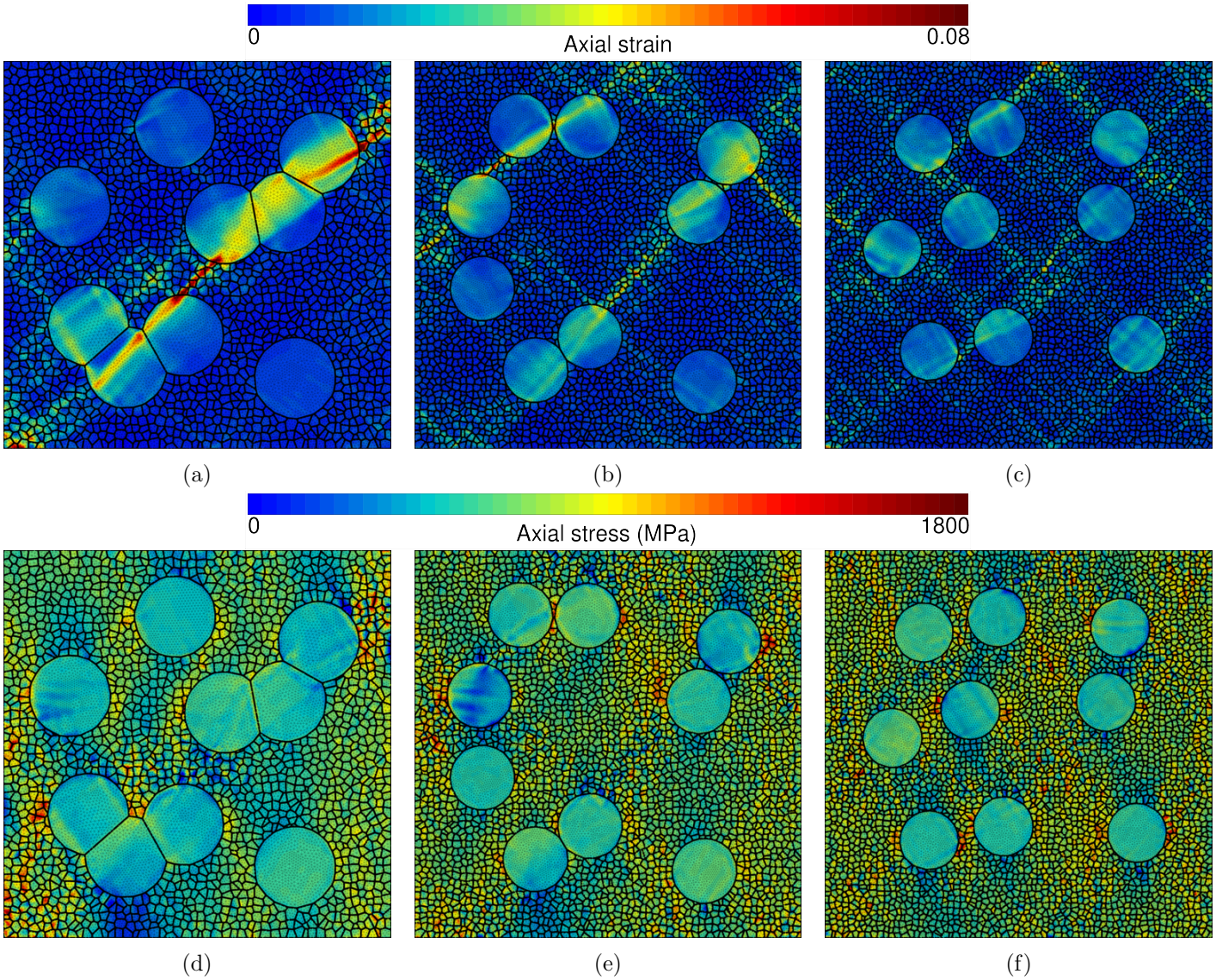

Figure 18: Influence of the CG distribution on the strain and stress fields, for a grain size ratio of 10: (a, d) Clusters, (b, e) Groups and (c, f) Isolated. The size of FG is about 0.5 µm. The tensile direction is vertical.

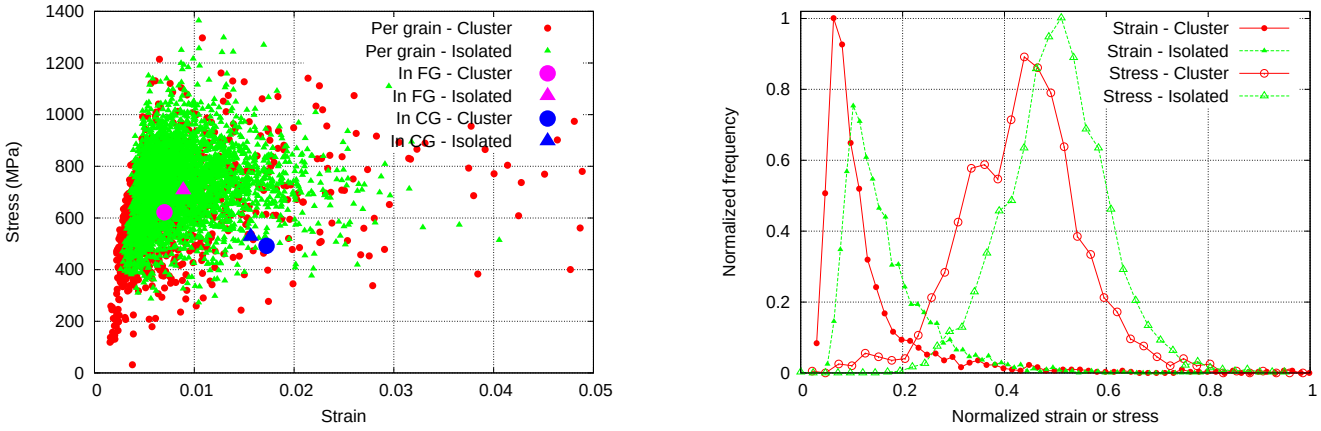

(a) (b)

Figure 19: Influence of the CG distribution on the mean responses per grain, for a grain size ratio of 10 and comparing the cases of isolated or clustered CG: (a) Axial stress-strain responses at 1% axial strain (b) the corresponding probability density functions (they have been normalized for the sake of visualization in a single diagram). The size of FG is about 0.5 µm.

5. Conclusion

The deformation of bimodal polycrystals, which include two populations of grains of distinctly different sizes, was analysed in detail. Focus was made on the simulations conditions (2D vs 3D, boundary conditions, etc.) and on the macroscopic and local deformations. The main results are:

- 2D-extruded polycrystals with "flat and parallel" boundary conditions along the extrusion direction can be used instead of 3D polycrystals for a semi-quantitative analysis and reasonable computation times.
- A complex interplay between FG and CG was observed in the model case of a single CG embedded in a FG matrix: the crystallographic nature of each constituent can affect significantly the development of intragranular heterogeneities, concerning either the localisation patterns or the statistical distributions.
- A minimum of 9 CG in the polycrystal are needed to obtain representative macroscopic properties (in the ranges of GS and GS ratios considered in this study).
- Both the grain size distributions and the CG spatial distribution (isolated or clustered) are shown to play a major role on the local response and on the effective constitutive behavior.

In the case of CG clusters, deformation bands appear: they initiate inside CG and propagate from cluster to cluster along directions of maximal shear oriented at 45° with respect to the tensile direction. Local stresses tend to concentrate at CG/FG interfaces, perpendicularly to the tensile direction, where the strain incompatibilities between CG and the FG matrix are the highest. This effect of stress concentrations at the interfaces is even more pronounced in the case of isolated CG. Stress relaxation channels are also observed between CG, along the tensile direction, which confirms previous experimental observations [20]. The presence of CG or CG clusters, by localising deformation, enables a stress relaxation in bimodal polycrystals, as compared to their unimodal FG counterparts.

Acknowledgements
The french region Normandie and the European Community are acknowledged for their financial support in the frame of the CPER project SUPERMEN.

References

[1] L. Méric, G. Cailletaud, M. Gaspérini, F.e. calculations of copper bicrystal specimens submitted to tension-compression tests, Acta Metall. Mater. 42 (3) (1994) 921–935.

[2] E. Hall, The deformation and ageing of mild steel: III discussion of results, Proc. Phys. Soc. Section B 64 (9) (1951) 747–753.

[3] N. Petch, The cleavage strength of polycrystals, J. Iron Steel Inst. 173 (1953) 25–27.

[4] H. Gleiter, Nanocrystalline materials, Prog. Mater. Sci. 33 (4) (1989) 223–315.

[5] M. Meyers, A. Mishra, D. Benson, Mechanical properties of nanocrystalline materials, Prog. Mater. Sci. 51 (4) (2006) 427–556.

[6] A. Pineau, A. Benzerga, T. Pardoen, Failure of metals III: Fracture and fatigue of nanostructured metallic materials, Acta Mater. 107 (2016) 508–544.

[7] C. Keller, K. Tabalaiev, G. Marnier, J. Noudem, X. Sauvage, E. Hug, Influence of spark plasma sintering conditions on the sintering and functional properties of an ultra-fine grained 316l stainless steel obtained from ball-milled powder, Mater. Sci. Engng A 665 (2016) 125–134.

[8] E. Ma, Eight routes to improve the tensile ductility of bulk nanostructured metals and alloys, JOM 58 (4) (2006) 49–53.

[9] L. Lu, Ultrahigh strength and high electrical conductivity in copper, Science 304 (5669) (2004) 422–426.

[10] C. Koch, Optimization of strength and ductility in nanocrystalline and ultrafine grained metals, Scripta Mater. 49 (7) (2003) 657–662.

[11] S. Cheng, Y. Zhao, Y. Zhu, E. Ma, Optimizing the strength and ductility of fine structured 2024 al alloy by nano-precipitation, Acta Mater. 55 (17) (2007) 5822–5832.

[12] E. Ma, Instabilities and ductility of nanocrystalline and ultrafine-grained metals, Scripta Mater. 49 (7) (2003) 663–668.

[13] G. Dirras, J. Gubicza, S. Ramtani, Q. Bui, T. Szilágyi, Microstructure and mechanical characteristics of bulk polycrystalline ni consolidated from blends of powders with different particle size, Mater. Sci. Engng A 527 (4-5) (2010) 1206–1214.

[14] Z. Zhang, S. Vajpai, D. Orlov, K. Ameyama, Improvement of mechanical properties in SUS304l steel through the control of bimodal microstructure characteristics, Mater. Sci. Engng A 598 (2014) 106–113.

[15] H. Azizi-Alizamini, M. Militzer, W. Poole, A novel technique for developing bimodal grain size distributions in low carbon steels 57 (2007) 1065–1068.

[16] M. Papa Rao, V. Subramanya Sarma, S. Sankaran, Processing of Bimodal Grain-Sized Ultrafine-Grained Dual Phase Microalloyed V-Nb Steel with 1370 MPa Strength and 16 pct Uniform Elongation Through Warm Rolling and Intercritical Annealing, Metall Mater Trans A 45 (12) (2014) 5313–5317.

[17] B. Flipon, L. Garcia de la Cruz, E. Hug, C. Keller, F. Barbe, Elaboration of austenitic stainless steel with bimodal grain size distribution and investigation of their mechanical behavior, 20th Int. ESAFORM Conf. on Material Forming, 26-28 April 2017, Dublin, Ireland, AIP Conference Proceedings 1896, 200007, 2017.

[18] S. Shekhar, J. Cai, , J. Wang, M. Shankar, Multimodal ultrafine grain size distributions from severe plastic deformation at high strain rates, Mater. Sci. Engng A 527 (2009) 187–191.

[19] K. Kurzydłowski, J. Bucki, Flow stress dependence on the distribution of grain size in polycrystals, Acta Metall. Mater. 41 (11) (1993) 3141–3146.

[20] B. Flipon, C. Keller, L. G. de la Cruz, E. Hug, F. Barbe, Tensile properties of spark plasma sintered AISI 316L stainless steel with unimodal and bimodal grain size distributions, Mater. Sci. Engng A 729 (2018) 249–256.

[21] S. Joshi, K. Ramesh, B. Han, E. Lavernia, Modeling the Constitutive Response of Bimodal Metals, Metall Mater Trans A 37 (2006) 2397–2404.

[22] B. Zhu, R. Asaro, P. Krysl, K. Zhang, J. Weertman, Effects of grain size distribution on the mechanical response of nanocrystalline metals: Part II, Acta Mater. 54 (2006) 3307–3320.

[23] L. Zhu, J. Lu, Modelling the plastic deformation of nanostructured metals with bimodal grain size distribution, Int. J. Plasticity 30-31 (2012) 166–184.

[24] G. Weng, The overall elastoplastic stress-strain relations of dual-phase metals, J. Mech. Phys. Sol. 38 (3) (1990) 419–441.

[25] S. Berbenni, V. Favier, M. Berveiller, Impact of the grain size distribution on the yield stress of heterogeneous materials, Int. J. Plasticity 23 (1) (2007) 114–142.

[26] G. Weng, A micromechanical theory of grain-size dependence in metal plasticity, J. Mech. Phys. Sol. 31 (3) (1983) 193–203.

[27] S. Ramtani, H. Bui, G. Dirras, A revisited generalized self-consistent polycrystal model following an incremental small strain formulation and including grain-size distribution effect, Int. J. Engng Sci. 47 (4) (2009) 537–553.

[28] J. Pipard, N. Nicaise, S. Berbenni, O. Bouaziz, M. Berveiller, A new mean field micromechanical approach to capture grain size effects, Comput. Mater. Sci. 45 (3) (2009) 604–610.

[29] V. Taupin, S. Berbenni, C. Fressengeas, O. Bouaziz, On particle size effects: An internal length mean field approach using field dislocation mechanics, Acta Materialia 58 (16) (2010) 5532 – 5544. doi:https://doi.org/10.1016/j.actamat.2010.06.034.
URL http://www.sciencedirect.com/science/article/pii/S135964541000399X

[30] V. Taupin, R. Pesci, S. Berbenni, S. Berveiller, R. Ouahab, O. Bouaziz, Lattice strain measurements using synchrotron diffraction to calibrate a micromechanical modeling in a ferritecementite steel, Materials Science and Engineering: A 561 (2013) 67 – 77. doi:https://doi.org/10.1016/j.msea.2012.10.086.
URL http://www.sciencedirect.com/science/article/pii/S0921509312015213

[31] H. Chang, N. Cordero, C. Déprés, M. Fivel, S. Forest, Micromorphic crystal plasticity versus discrete dislocation dynamics analysis of multilayer pile-up hardening in a narrow channel, Arch. Appl. Mech. 86 (2016) 21–38.

[32] A. Magee, L. Ladani, Representation of a microstructure with bimodal grain size distribution through crystal plasticity and cohesive interface modeling, Mech Mater 82 (2015) 1–12.

[33] B. Flipon, L. Milhem, C. Keller, R. Quey, F. Barbe, Modelling of polycrystals using well-controlled Voronoi-type tessellations and its applications to micromechanical analyses, Presse des Mines, 2018, Ch. 23, pp. 187–198, physics and Mechanics of Random Media: from Morphology to Material Properties.

[34] I. Benedetti, F. Barbe, Modelling Polycrystalline Materials: An Overview of Three-Dimensional Grain-Scale Mechanical Models, Journal of Multiscale Modelling 5 (2013) 1–51.

[35] R. Quey, L. Renversade, Optimal polyhedral description of 3d polycrystals: Method and application to statistical and synchrotron x-ray diffraction data, Comput. Meth. Appl. Mech. Engng 330 (2018) 308–333.

[36] R. Quey, P. Dawson, F. Barbe, Large-scale 3d random polycrystals for the finite element method: generation, meshing and remeshing, Comput. Meth. Appl. Mech. Engng 200 (17-20) (2011) 1729–1745.

[37] F. Lavergne, R. Brenner, K. Sab, Effects of grain size distribution and stress heterogeneity on yield stress of polycrystals: A numerical approach, Comput. Mater. Sci. 77 (2013) 387–398.

[38] V. Phan, T. Nguyen, Q. Bui, G. Dirras, Modelling of microstructural effects on the mechanical behavior of ultrafine-grained nickel using crystal plasticity finite element model, Int. J. Engng Sci. 94 (2015) 212–225.

[39] S. Forest, Micromorphic approach for gradient elasticity, viscoplasticity, and damage, Journal of Engineering Mechanics 135 (2009) 117–131.

[40] N. Cordero, A. Gaubert, S. Forest, E. Busso, F. Gallerneau, S. Kruch, Size effects in generalised continuum crystal plasticity for two-phase laminates, J. Mech. Phys. Sol. 58 (11) (2010) 1963–1994.

[41] S. Wulfinghoff, T. Böhlke, Equivalent plastic strain gradient enhancement of single crystal plasticity: theory and numerics, Proceedings of the Royal Society of London A: Mathematical, Physical and Engineering Sciences 468 (2145) (2012) 2682–2703.

[42] C. Keller, E. Hug, A. Habraken, L. Duchene, Finite element analysis of the free surface effects on the mechanical behavior of thin nickel polycrystals, Int. J. Plasticity 29 (2012) 155–172.

[43] P. Franciosi, The concepts of latent hardening and strain hardening in metallic single crystals, Acta Metall. 33 (9) (1985) 1601–1612.

[44] C. Gérard, G. Cailletaud, B. Bacroix, Modeling of latent hardening produced by complex loading paths in fcc alloys, Int. J. Plasticity 42 (2013) 194–212.

[45] F. Barbe, R. Quey, A. Musienko, G. Cailletaud, Three-Dimensional characterization of strain localization bands in a high-resolution elastoplastic polycrystal, Mech. Res. Com. 36 (2009) 762–768.

[46] F. Barbe, S. Forest, G. Cailletaud, Intergranular and intragranular behavior of polycrystalline aggregates. part 2: Results, Int. J. Plasticity 17 (4) (2001) 537–563.

[47] C. Keller, E. Hug, X. Feaugas, Microstructural size effects on mechanical properties of high purity nickel, Int. J. Plasticity 27 (4) (2011) 635–654.

[48] H. Moulinec, P. Suquet, A numerical method for computing the overall response of nonlinear composites with complex microstructure, Comput. Meth. Appl. Mech. Engng 157 (1) (1998) 69–94.

[49] P. Doumalin, M. Bornert, J. Crépin, Characterisation of the strain distribution in heterogeneous materials, Mécanique & Industries 4 (2003) 607–617.